RSC Advances

ROYAL SOCIETY OF CHEMISTRY

www.rsc.org/advances

RSC Advances

RSCPublishing

COMMUNICATION

Functionalized Carbon Microarrays Platform for High Sensitive Detection of HIV-Tat Peptide

Cite this: DOI: 10.1039/x0xx00000x

Varun Penmatsa,[a,b*] Ruslinda A. Rahim,[c] Hiroshi Kawarada,[d] and Chunlei Wang [a]

Received 00th January 2015,
Accepted 00th January 2015

DOI: 10.1039/x0xx00000x

www.rsc.org/

The detection of HIV disease at an early stage has significant clinical implication. We report the detection of HIV-TAT peptide on functionalized three-dimensional carbon micropillar array platform. The sensor showed linear relationship between HIV-TAT concentration and fluorescence intensity in the sub-nanomolar range with a detection limit of 50 pmol.

INTRODUCTION

Diagnosis of HIV infection at an early stage is of great significance to ensure that patients can be promptly provided treatment and enrolled into related support services to help them reduce the risk of new HIV transmissions. HIV-1 Tat is a 86 - 101 residue protein that is typically produced very early during the infection and regulates early stages of the HIV life cycle [1,2]. TAT peptides, which are typically composed of 49-57 amino acids, are an important constituent of the HIV-1 TAT protein that is responsible for TAT protein translocation [3,4]. In addition to the regulation of HIV life cycle, Tat peptide is believed to onset several AIDS-associated pathologies by targeting both infected and uninfected cell types [3]. Previous report has shown that at least two-third of the produced Tat protein is released extracellularly from an infected cell [4]. Extracellular Tat targets different types of non-HIV permissive cells exerting a wide array of biological activities such as modulation of cytokine/receptor expression, proliferation, cell migration, apoptosis and differentiation [3]. These processes contribute to the onset of the clinical disorders including central and peripheral neuropathies, early lymph node hyperplasia followed by lymphoid depletion, pulmonary complications, vasculopathies, nephritis, heart disease, and an increased incidence of cancerous tumors [2]. With evidence that Tat can be detected in the serum of HIV-infected individuals, a series of studies have been devoted to the detection of HIV-1 TAT peptide as a potential biomarker for early detection of AIDS [5-8,41].

Recent studies have demonstrated aptamer- based HIV-1 Tat peptide detection using optical, microbalance and potentiometric methods [5-8]. Aptamers, essentially are single-stranded DNA or RNA molecules that are selected and amplified from synthetic nucleic acid libraries [9-11]. Yamamoto et al. developed an aptamer that yielded an efficient binding specificity against Tat but not for other cellular factors [12]. The previous HIV-Tat biosensing on solid platforms using gold [5], carbon nanostructures [41], and diamond substrates [7] have showed good sensitivity, but the material cost, controllability of defects and grain boundaries in polycrystalline diamond substrates along with the high operating cost due to the need for high vacuum and high temperature systems are limiting factors for mass production.

On the other hand, microfabrication of carbonaceous material using Carbon-Microelectromechanical (C-MEMS) process which is based on the thermochemical decomposition of patterned organic photoresist at high temperatures in oxygen-free atmosphere has garnered wide spread attention [13-18]. By changing the lithography processing conditions and pyrolysis parameters, a wide variety of carbon structure with different crystallinity, shape and size can be fabricated. Additionally, integrating nanomaterials (such as graphene [13], carbon nanotubes [14,15], nanofibers [16,17]) to these high surface area carbon microarray platform links the micro and nano-scale carbon structures, showing great potential in achieving whole carbon electronics. In addition, Pyrolyzed photoresist carbon electrodes exhibit better resistance towards biofouling, easy surface modification and functionalization, superior chemical stability, and comparable reaction kinetics to glassy carbon but with lower oxygen/carbon atomic (O/C) ratio. [18-23].

In this work, the feasibility of vacuum ultraviolet pretreatment for the surface functionalization of pyrolyzed carbon surface has been demonstrated. To the best of our knowledge, this is the primary work that demonstrates VUV pretreatment for the biofunctionalization of pyrolyzed photoresist carbon surface that is used in biosensing application. In addition, for the first time, the functionalized high surface area C-MEMS platform has been demonstrated for high sensitive detection of HIV-1 TAT protein using RNA aptamers. The sensitivity and the reproducibility of the carbon micropillar array platform for HIV-1 TAT peptide detection were evaluated.

EXPERIMENTAL DETAILS

Typical C-MEMS process was used for the fabrication of the three-dimensional carbon micropillar arrays. The C-MEMS process has been extensively discussed elsewhere [15, 18, 24, 25]. 4 inch silicon wafers were cleaned using acetone and methanol followed by a dehydration bake at 150 °C for 5 min on a hotplate. A 200 μm NANO™ SU-8 100 photoresist film was obtained by spin coating the photoresist at 500 rpm for 12sec and then 1200 rpm for 30sec. The photoresist was soft baked at 65 °C for 10 min and at 95 °C for 30 min. The photoresist was exposed for 60 sec (light intensity, 17mW/cm^2) using OAI Hybralign contact aligner to crosslink polymer chains in the photoresist. Post expose bake was carried out at temperatures of 65 °C for 1 min and 95 °C for 3 min and the patterned samples were developed using NANO™ SU-8 developer (Microchem, USA) for 15 min to wash away the unwanted photoresist. The carbonization of the photoresist micropillar arrays was conducted in a tube furnace under forming gas (95% N_2+ 5% H_2) environment with a hold time of 60 min.

The system used in this work used a xenon excimer (Xe) lamp to generate an ultraviolet (VUV) light with a central wavelength of 172 nm. After the sample was inserted, the chamber was evacuated and oxygen gas (O_2) was introduced until a pressure of 3.0×10^4 Pa was reached. VUV treatment was performed at 20 W lamp power and 12 mW/cm^2 of light intensity. The treatment time varies from 15 to 120 min. The whole treatment process was conducted at room temperature. The excimer light is transmitted through the glass window of the lamp housing and chemical reaction chains were triggered in the irradiation chamber. The working principle of the VUV surface treatment is extensively discussed in Ref 26.

Following the functionalization of the carbon surface, the covalent immobilization of RNA^{Tat} aptamer was performed on the carbon surface via amide chemistry. The probe RNA^{Tat} aptamer terminated on it 5' end with an amino group (NH2-3'-AAUACUUCGCUAGCUGGCU-5'), and the fluorescence-labeled RNA aptamer (Cy5-3'- AAGCCCUAGUUCGAAG-5') were purchased from Sigma Genosys Japan (Hokkaido, Japan). The HIV-1 TAT (HIV-1 Tat-derived peptide; amino acids 49-57) was purchased from Immuno Diagnostics, Inc., and stored at -75 °C. Each sample was first treated with a 1:1 mixture of 0.1 M N-hydroxysuccinimide (NHS) and 0.4 M 1-ethyl-3-(3-dimethylaminopropyl) carbodiimide hydrochloride (EDC) for 1 hr to activate the carboxylic functional groups. To optimize the probe aptamer concentration, we have used different concentrations of probe aptamer starting from 5μM to 100μM. We found that as the probe aptamer concentration increased from 5μM to 20μM there was increase in the resultant fluorescence intensity respectively but after 20μM there no considerable increase in the fluorescence intensity values and was within the error bar range even when the probe aptamer concentration was further increased. This could be attributed to the saturation of surface terminal groups and steric effect from the probe aptamers [20]. For this reason in our work we have fixed the probe aptamer concentration as 20μM. The probe RNATat aptamer was prepared by diluting with 3× sodium saline citrate (SSC), 0.1 M NHS and 0.4 M EDC, to a final concentration of 20 μM, and small droplets of the solution were again deposited manually on the surface. Each sample was incubated at 38 °C for 2 h in a humidified chamber, which was followed by thorough rinsing with PBS with Tween-20 (0.1% Tween-20). The binding of HIV-1 Tat protein with the immobilized probe RNA^{Tat} aptamer were performed at room temperature for 1 hr. The concentration of HIV-1 Tat protein was 100 nM in 2× SSC buffer solution. Following Tat protein binding, the aptamer-derived second strand was introduced to the target for 1 hr at room temperature. The concentration of the second strand of aptamer was 1μM in 2× SSC buffer solution. The sample was then rinsed with Tris–HCl buffer solution for 7 min to avoid nonspecific binding. To remove the Tat protein to achieve the regeneration process, urea (8.3 M) solution was used for washing for around 10mins.

The morphology of 3D carbon microarrays was investigated using JOEL 6335 FE- SEM scanning electron microscopy. The chemical composition of pyrolyzed photoresist carbon film before and after d1irect amination procedure was investigated by an Ulvac Φ 3300 x-ray photoelectron spectroscopy (XPS) with an anode source providing Al Kα radiation. The electron takeoff angle was 45±3° relative to the substrate surface. Fluorescence observation was performed using an Olympus IX71 epifluorescence microscope.

RESULTS AND DISCUSSION

The microstructural and electrical properties of C-MEMS based carbon have been extensively characterized in our previous publications [24, 27]. A typical SEM image of high aspect ratio 3D carbon micropillar arrays is shown in Figure S1. The average dimensions of the carbon micropillars after carbonizing patterned SU-8 photoresist structures are ~ 160μm height and ~ 30μm width. By changing the mask design, processing conditions during spin coating and photolithography, the height and width of the individual pillars can be easily controlled.

In order to covalently immobilize probe RNA aptamer on the carbon surface, it is essential to biofunctionalize the carbon surface. For this reason, the sample was pretreated by vacuum-ultraviolet (VUV) pretreatment. In this functionalization technique, a xenon excimer (Xe) lamp with a central wavelength of 172 nm generates an ultraviolet (VUV) light, which triggers chemical reaction chains. The reactions at the atomic and molecular level responsible for excimer and excited oxygen generation are

$$Xe^*_2 \rightarrow Xe + Xe + h\nu \quad (1)$$

followed by

$$O_2 + h\nu \rightarrow 2O \quad (2)$$

$$O_2 + O \rightarrow O_3 \quad (3)$$

$$2O_3 + h\nu \rightarrow 3O_2 \quad (4)$$

The high density ozone and excited oxygen are the primary agents that functionalize the carbon surface by oxidizing the surface and introducing –COOH with other functional groups. The energy of photons at 172-nm wavelength is 697.5 kJ/mol, so VUV treatment with these photons can break molecular bonds with bond energies up to 697.5 kJ/mol. Most of the bond energies of molecules with carbon are lower than of the VUV photon energy. When O2 is introduced into the chamber for the VUV/O3 treatment, the excimer light interacts with the oxygen, and results in the generation of ozone (O3) and excited oxygen radicals O (1D). The high density ozone and excited oxygen are the primary agents that functionalize the carbon surface by oxidizing the surface and introducing –COOH with other functional groups. The excited oxygen also aids in breaking the chemical bonds quickly and efficiently [28].

The major advantage of using VUV pretreatment compared to majority of other surface treatments is that VUV surface treatment being a photochemical oxidation technique avoids direct contact of the plasma with the sample surface, reducing the damage caused through etching of carbon atoms and at the same time maintains the primary advantage of plasma functionalization being solvent-free dry process. On the other hand, other oxidation pretreatment techniques can extensively damage the structural integrity and significantly modify the electrode morphology due to exposure to high-energy species such as electrons or ions, often generated in discharge plasmas.

The elemental composition and surface binding of pyrolyzed photoresist film were evaluated by X-ray photoelectron spectroscopy spectra (XPS) as shown in Figure 1a. The carbon and oxygen peak for both bare carbon and VUV treated carbon surface in typical XPS broad scan spectra can be compared. The small peak in the XPS spectrum for bare carbon represents the native surface carbon-oxygen bonds. After oxidation with VUV pretreatment, it can be observed that the oxygen peak is more apparent and this indicates preeminent surface oxidation using VUV pretreatment. The measured oxygen content or O/C ratio, which quantifies the surface oxidation, is calculated from these broad scan XPS spectra by dividing the peak intensity of oxygen with peak intensity of carbon. The peak intensity was determined by integrating the area under the corresponding peak in the XPS spectrum. The summary of measured oxygen content as a function of oxidation time in the case of VUV (Figure 1b), and analysis of the graph shows that the achievable oxidation levels (O/C ratio) on carbon surface was ~7 at.% for the untreated carbon surface but increases to ~24 at.% after treating the carbon surface with 75mins of VUV treatment. The ~350% increase in the O/C ratio is a clear indication of the oxidation of the carbon surface with results in different carbon-oxygen based functional groups such as carboxyl, carbonyl, etc. The oxygen content values shown in the graph are an average of three readings for each functionalization time. It should be noted that the obtained oxygen coverage using VUV is considerably higher or comparable to most other oxidation techniques reported in the literature [29-36].

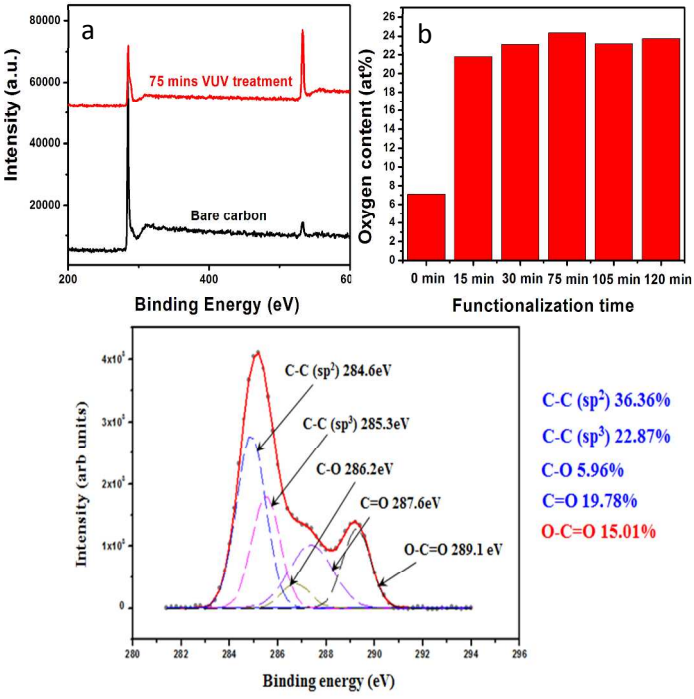

Figure 1: (a) Broadscan X-ray photoelectron spectroscopy spectra comparing bare carbon and VUV pretreated carbon film for 75 min; (b) Relationship of oxygen concentration (at%) and VUV pretreatment times; (c) Deconvoluted C1s spectra of pyrolyzed carbon film after 75mins VUV pretreatment. Here solid line shows the original data and dashed lines show the fitting curves.

A high resolution C1s XPS spectrum of pyrolyzed carbon surface treated by VUV technique is shown in Figure 1c. Due to the rather broad individual contributions (FWHM typically 1 eV) the C1s peak can be decomposed into various components. The following 5 peaks can be deconvoluted: C-C (sp2) at 284.6 eV, C-C (sp3) at 285.3 eV, C+ I (C-O) at 286.2 eV, C+ II (C=O) at 287.6 eV and C+ III (O-C=O) at 289.1 eV. The primary functional group we are interested in this study is O-C-OH, which can be used to bind covalently with amine-terminated biomolecules. The peak of carboxyl group is strong in VUV and one common trend that can be observed is that upon oxidation the sp^2 contents decrease steadily while the oxygen-related components gain in intensity. The coverage of the carboxyl group on the surface reached close to 15% in the case of VUV The reason why we did not get further surface coverage could be due to the steric limitations that limit amine group coverage on the surface to a certain level. Ideally, quantification of the effectiveness of aptamer immobilization is most valuable. However, it should be noted that the 15% distribution of carboxyl groups on the carbon surface obtained in our work is a functional indicator of the sensing surface available for binding of the amino terminated probe aptamers. In our future work we will focus on developing a suitable technique to quantify the immobilization efficiency that takes into account of the spatial variances in the immobilization across the 3D electrode surface.

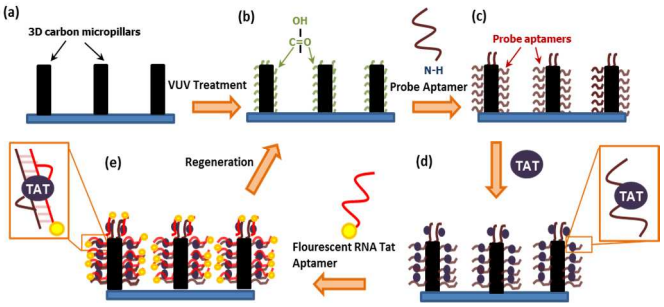

Figure 2: Schematic illustration of the detection of HIV-TAT peptide using RNA aptamers on 3D carbon microarrays platform; (a) bare carbon micropillar platform, (b) surface functionalization of the carbon surface using VUV pretreatment, (c) covalent immobilization of the probe RNA aptamer, (d) intercalating the HIV-TAT peptide to the probe aptamer (e) binding of the fluorescence labelled RNA Tat aptamer with the probe RNA aptamer forming a duplex with Tat peptide in between.

Figure 2 depicts the aptamer-based detection mechanism on HIV 1 Tat peptide protein. After functionalizing the 3-D C-MEMS micropillars platform with VUV treatment, the amino-terminated probe RNA^{Tat} aptamers are immobilized on the carboxylated carbon micropillar surface via amide chemistry. The Tat peptides are then introduced to bind with the probe aptamers. In the next step, fluorescently tagged RNA aptamers that are highly specific to the Tat peptides are introduced. In the

presence of Tat peptides, the two RNA aptamers undergo a conformational change to form a duplex in which a significant enhancement of detectable fluorescence. It is important to note that without the presence of TAT peptide, the probe RNA^{Tat} aptamers and fluorescently tagged RNA aptamers cannot bind, and thus no detectable fluorescence from the sample.

Quantitative fluorescence measurements were analyzed between the immobilized probe RNA^{Tat} aptamer and Tat peptide in a wide range concentration of 50 pM-100 nM. After the binding of the fluorescence tagged RNA aptamer to the probe RNA^{Tat} aptamer with Tat peptide sandwiched in between, the fluorescence intensity values were measured by taking the average value of nine top-view fluorescence images of the micropillars. Figure 3(a) shows a relationship between tat peptide concentration and the relative increase in the fluorescence signal that was observed. It should be noted that different carbon micropillars samples shows slightly different base fluorescence intensity. In order to better compare the sensing effect, in Figure 3a, the y-axis values which represent the change in the fluorescence intensity at different concentrations were normalized for easy representation. The results show that from 50pM-100nM there is a near-linear relationship between the HIV-TAT concentration and the fluorescence intensity values. The fluorescence intensity value for blank control sample was miniscule and close to the detection baseline. The detection limit of 50 pM is beyond the typical concentration of 0.1-1nM found in HIV infected patient. The excellent detection limit could be attributed to the fact that 3D micropillar arrays do not suffer from optical interference obtained on oxidized silicon substrates compared to fluorescence detection on 2D micropatterns fabricated on SiO_2/Si substrate [20]. It has been previously shown that the phenomena of modulating fluorescence intensity by using optical interferences leads to strong fluorescence from unbinded flouropore on the SiO_2/Si substrate [37-39] which leads to strong optical intensity even from non-specific binded fluorescently tagged aptamers. Moreover, the measurements were performed repeatedly to confirm the high selectivity and detection sensitivity of Tat peptide on the carboxyl terminated carbon surface by fluorescence observation. The concentration used during the regeneration test was 0.1nm. The detection system can be regenerated very efficiently using 8.3 M urea solution to denature the protein, by breaking the hydrogen bonds, and remove it from the probe RNA^{Tat} aptamer. The rise in signal intensity was clearly observed upon fluorescence tagged RNA aptamer binding in the presence of TAT peptide and was significantly reduced after denaturation as shown in Fig. 3(b). Cyclical detection was performed for three cycles over 3 days without losing sensitivity. The reproducibility proved that RNA aptamers which are covalently immobilized on the carbon surface are robust acid and maintain their ability to bind selectively to Tat peptide after regeneration.

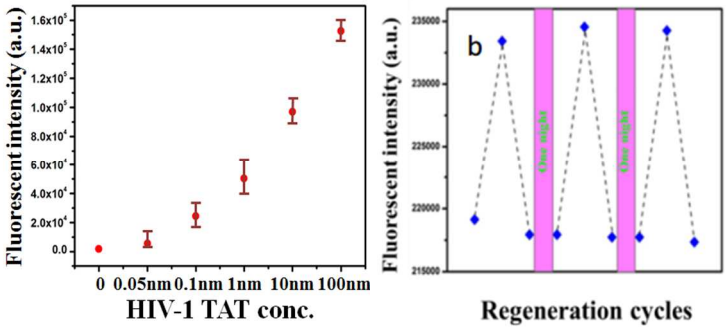

Figure 3: (a) Response of the sensing platform to different concentrations of TAT peptide from 0.05 nM to 100 nM. The concentrations of the probe aptamer and fluorescence tagged aptamer were 20 μM and 1 μM, respectively. (b) Reproducible detection of Tat peptide was performed for 3 cycles by regenerating the sensor platform using 8.3 M urea.

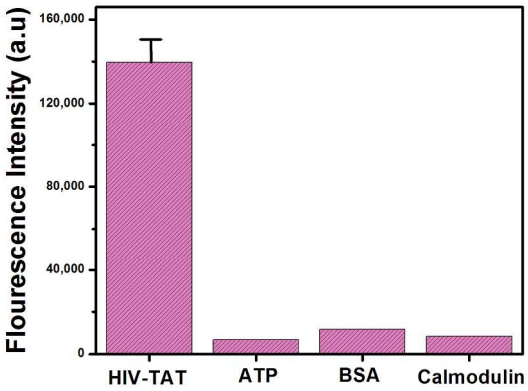

Figure 4: Selectivity study comparing fluorescence intensity of different proteins towards RNA^{Tat} aptamer. The concentration of the different molecules (TAT peptide, ATP, BSA and calmodulin) was 100 nM. The concentrations of the probe aptamer and fluorescence tagged aptamer were 20 μM and 1 μM, respectively.

Figure 4 shows the selectivity study of the sensing platform towards Tat peptide and three other biological components. Adenosine triphosphate and calmodulin are biomolecules which are abundantly present in the human blood and along with BSA which is a mixture of different proteins act as potential interferences for selective detection of target analyte in blood, in our case HIV-1 TAT peptide. The graph summarizes the fluorescence intensity when detecting each biological component. It can be clearly observed that the fluorescence intensity when detecting ATP, BSA and calmodulin is significantly lower than when detecting Tat peptide. This can be explained by the fact that the probe RNA^{Tat} aptamer has high affinity and selectivity towards the Tat peptide compared to other biological components. Even for BSA, which typically contains a high concentration of proteins, the probe RNA^{Tat} aptamer does not show selectivity towards it. With additional future work of using the sensing platform to detect Tat peptide from real HIV-infected person blood sample, there is potential to use the sensing platform in clinical applications. In addition, with the integration of nanomaterials such as graphene and CNTs on to the 3D micropillar arrays, there is an opportunity to further improve the sensitivity and selectivity of the detection platform.

The positive aspect of our work demonstrates: the feasibility of VUV treatment as a versatile technique for biofunctionalization of pyrolyzed carbon; the 3-D carbon micropillars arrays can be used as a highly sensitive detection platform for HIV-TAT peptide; the detection limit of 50pM shown by the sensor in this work is much lower than the extracellular HIV TAT found in the serum of AIDS patients ranges which is typically between 100pM- 1000pM [39].

Conclusions

In conclusion, VUV pretreatment has been shown to provide stable carboxylic terminated carbon surface with ≈ 24 at. %. The use of 3D carbon micropillars helped alleviate the optical interferences obtained on oxidized silicon substrates for 2D structures and thus was possible to achieve a notable detection limit of 50 pmol. The reusability of the sensing platform was demonstrated three times without any significant loss over a period of 3 days without any significant loss in the performance by regenerating the probe aptamer.

Acknowledgements

Varun Penmatsa gratefully acknowledges financial support from DEA and DYF fellowships provided by FIU graduate school. This project is partially supported by National Science Foundation (OISE 0934078 and CMMI 0800525) along with Grant-in-Aid from GCOE Research from the Ministry of Education, Culture, Sports, Science and Technology, Japan and a Grant-in-Aid for Fundamental Research A (23246069) of Japan Society for the Promotion of Science (JSPS). Ruslinda A. Rahim acknowledges funding from Research Acculturation Collaborative Effort (9017-00022), Ministry of Education, Malaysia and L'oreal Fellowship for Women in Science

Notes and references

[a] Department of Mechanical and Materials Engineering, Florida International University, Miami USA.
[b] Now at Department of Ophthalmology and Visual Science, The Ohio State University, Columbus USA.
[c] Institute of Nano Electronic Engineering (INEE), Universiti Malaysia Perlis, Jln seriab-Alor setar, 01000 Kangar, Perlis Malaysia.
[d] School of Science and Engineering, Waseda University, Ohkubo 3-4-1 Shinjuku 169-8555, Tokyo Japan.

Electronic Supplementary Information (ESI) available:

1 B. Ensoli, L. Buonaguro, G. Barillari, V. Fiorelli, R. Gendelman, R. A. Morgan, P. Wingfield, R. C. Gallo, J Virol., 1993, 67, 277.
2 Persistent Lack of Detectable HIV-1 Antibody in a Person with HIV Infection, Centre for Disease Control and Prevention (CDC), Mortality and Morbidity Weekly Report, Utah, USA, 1995.
3 B. Romani, S. Engelbrecht, R. H. Glashoff, J. General Virology, 2010, 91, 1.
4 D. Milani, M. Mazzoni, G. Zauli, C. Mischiati, D. Gibellini, M. Giacca, S. Capitani, AIDS, 1998, 12, 1275.
5 S. Tombelli, M. Minunni, E. Luzi, M. Mascini, Bioelectrochem., 2005, 67, 135.
6 A. R. Ruslinda, K. Tanabe, S. Ibori, X. Wang, H. Kawarada, Biosens Bioelectron., 2013, 40, 277.
7 A. R. Ruslinda, X. Wang, Y. Ishii, Y. Ishiyama, K. Tanabe, H. Kawarada, Appl. Phys. Lett., 2011, 99, 123702.
8 M. Famulok, G. Mayer, Accounts of Chem. Res., 2011, 44, 1349.
9 A. D. Ellington, J. W. Szostak, Nature, 1990, 346, 818.
10 D. L. Robertson, G. F. Joyce, Nature, 1990, 344, 467.
11 C. Tuerk, L. Gold, Science, 1990, 249, 505.
12 R. Yamamoto, T. Baba, P.K. Kumar, Genes Cells, 2000, 5, 389.
13 V. Penmatsa, T. Kim, M. Beidaghi, H. Kawarada, Z. Wang, L. Gu, C. Wang, Nanoscale, 2012, 4, 3673.
14 W. Chen, M. Beidaghi, V. Penmatsa, K. Bechtold, L. Kumari, W.Z. Li, C. Wang, Nanotechnology, IEEE Transactions on, 2010, 9, 734.
15 C. Wang, R.Zaouk, M. Madou, Carbon, 2006, 44, 3073.
16 G. Canton, T. Do, L. Kulinsky, M. Madou, Carbon, 2014, 71, 338.
17 S. Sharma, A. Sharma, Y. K. Cho, M. Madou, ACS Appl. Mater. Inter., 2012, 4, 34.
18 S. Ranganathan, R. McCreery, S. Majji, M. Madou, J. Electrochem. Soc., 2000, 147, 277.
19 V. Penmatsa, H. Kawarada, Y. Song, C. Wang, Mater. Sci. Res. India, 2014, 11, 1.
20 V. Penmatsa, AR. Ruslinda, M. Beidaghi, H. Kawarada, C. Wang, Biosens Bioelectron., 2013 39, 118.
21 V. Penmatsa, J. H. Yang, Y. Yu, C. Wang, Carbon, 2010, 48, 4109.
22 V. Penmatsa; A.R. Ruslinda; M. Beidaghi; H. Kawarada; C. Wang, ECS Trans. 2013, 45, 7.
23 JH. Yang, V. Penmatsa, S. Tajima, H. Kawarada, C. Wang, Mater. Lett., 2009, 63, 2680.
24 C. Wang, G. Jia, L. H. Taherabadi, M. J. Madou, J. Microelectromech. Syst., 2005, 14, 348.
25 B. Park, L. Taherabadi, Ch. Wang, J. Zoval, M. Madou. J Electrochem. Soc., 2005, 152, J136.
26 H. Shinohara, T. Kasahara, S. Shoji, J. Mizuno, J. Micromech. Microeng., 2011. 21, 085028.
27 V. Penmatsa, H. Kawarada, C. Wang, J. Micromech. Microeng., 2012, 22, 045024.
28 K. Sakuma, J. Mizuno, N. Nagai, N. Unami, S. Shoji, IEEE Trans. On Electronic Packaging Manufacturing, 2010, 33, 212.
29 X. Wang X, R. Ruslinda, Y. Ishiyama, Y. Ishii, H. Kawarada, Diam Relat Mater., 2010, 20, 1319.
30 W. Wang W, B. Huang, L. Wang, D. Ye, Surf. Coat. Tech., 2001, 205, 4896.
31 P. Pehrsson, T. Mercer, Surf Sci., 2000, 460, 74.
32 S. Ferro, M. Colle, A. Battisti, Carbon, 439, 1191 (2005).
33 J. Nakamura, T. Ito, Appl Surf Sci., 2005, 244, 301.
34 R. Boukherroub, X. Wallart, S. Szunerits, B. Marcus, P. Bouvire, M. Mermoux, Electrochem comm., 1997, 7, 937.
35 C. Goeting, F. Marken, A. Gutierrez-Sosa, R. Compton, J. Foord, Diam Relat Mater., 2000, 9, 390.
36 H. Notsu, I. Yagi, T. Tatsuma, D. Tryk D, A. Fujishima, Electrochem. Solid-State Lett., 1999, 2, 522.
37 M. Bras, V. Dugas, F. Bessueille, J.P. Cloarec, J.R. Martin, M. Cabrera, J.P. Chauvet, E. Souteyrand, M. Garrigues, Biosens and Bioelec., 2004, 20, 797.
38 C. Oillic, P. Mur, E. Blanquet, G. Delapierre , F. Vinet, T. Billon, Biosens and Bioelec., 2007, 22, 2086.
39 A. Lambacher, P. Fromherz, Appl. Phys. A, 1996, 63, 207.
40 D. Milani, M. Mazzoni, G. Zauli, C. Mischiati, D. Gibellini, M. Giacca, S. Capitani, AIDS, 1998, 12, 1275.

41 A. R. Ruslinda, M. K. Md Arshad, S. Norhafizah, M.A. Farehanim, R.M. Ayub, U. Hasim, IEEE Conf. on Biomedical Engineering and Sciences, 2014, 840-844

